Supporting Information

Induction Heating Induced Self-Healing of Nanocomposites Based on Surface-Functionalized Cationic Iron Oxide Particles and Polyelectrolytes

Bastian Oberhausen, Guido Kickelbick

Inorganic Solid-State Chemistry, Saarland University, Campus C41, 66123 Saarbrücken, Germany

E-mail: guido.kickelbick@uni-saarland.de

Content

1. NMR and FTIR spectra of the cationic organophosphorus coupling molecule and its precursors

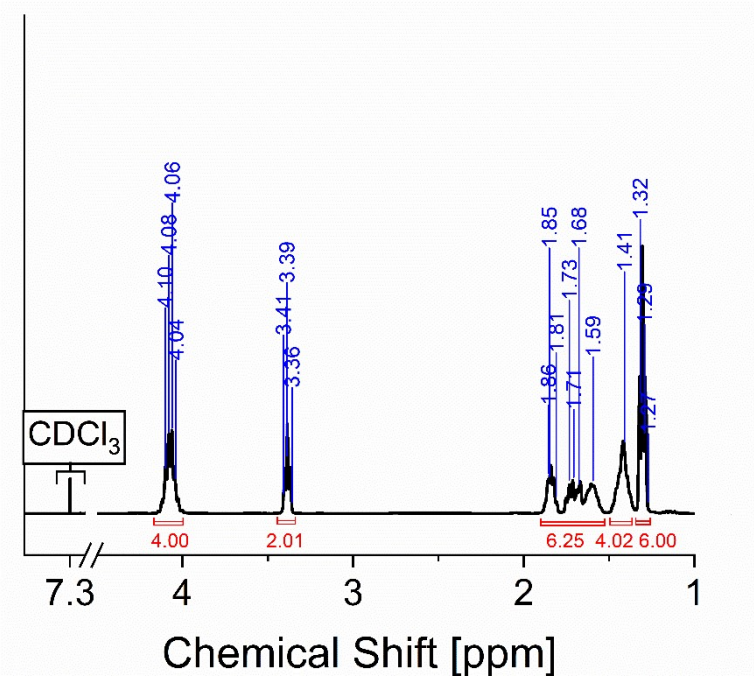

Figure S1: ^{1}H NMR spectrum of diethyl(6-bromohexyl) phosphonate.

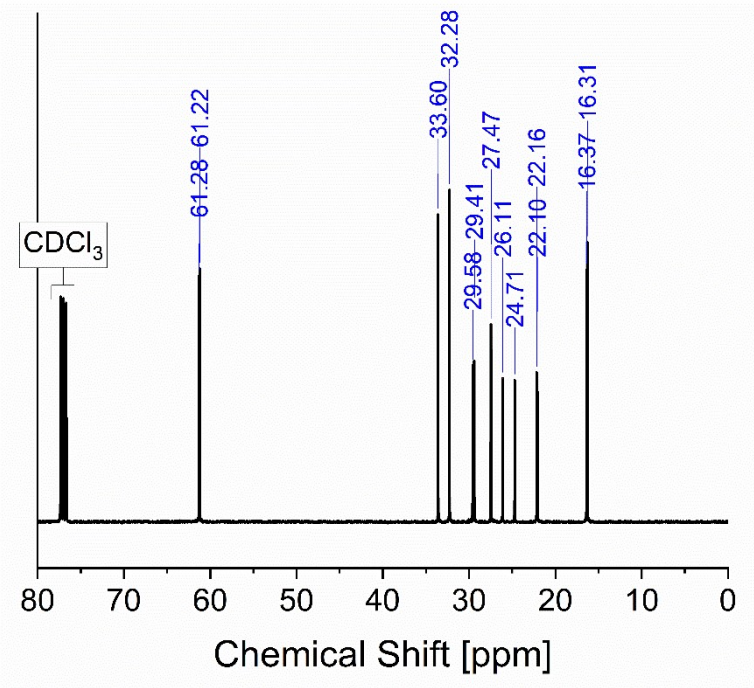

Figure S2: ^{13}C NMR spectrum of diethyl(6-bromohexyl) phosphonate

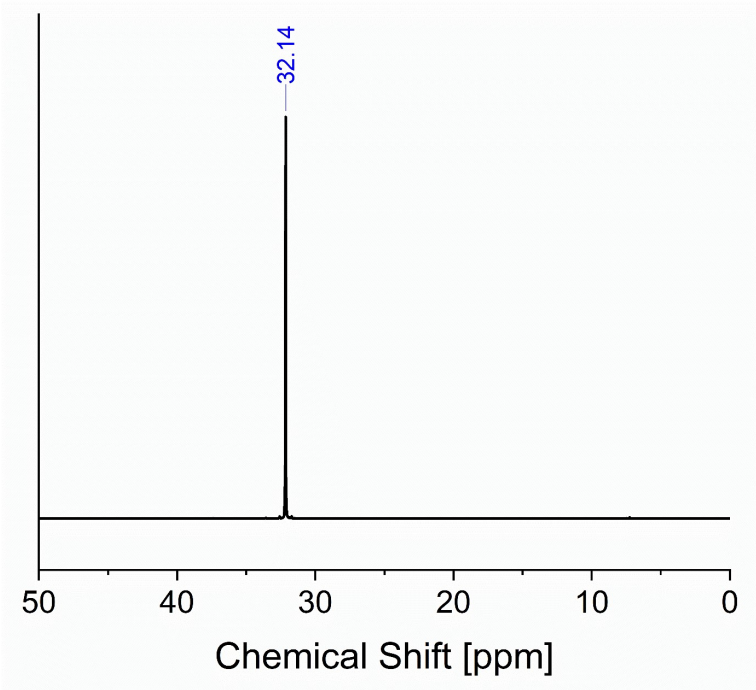

Figure S3: ^{31}P NMR spectrum of diethyl(6-bromohexyl) phosphonate.

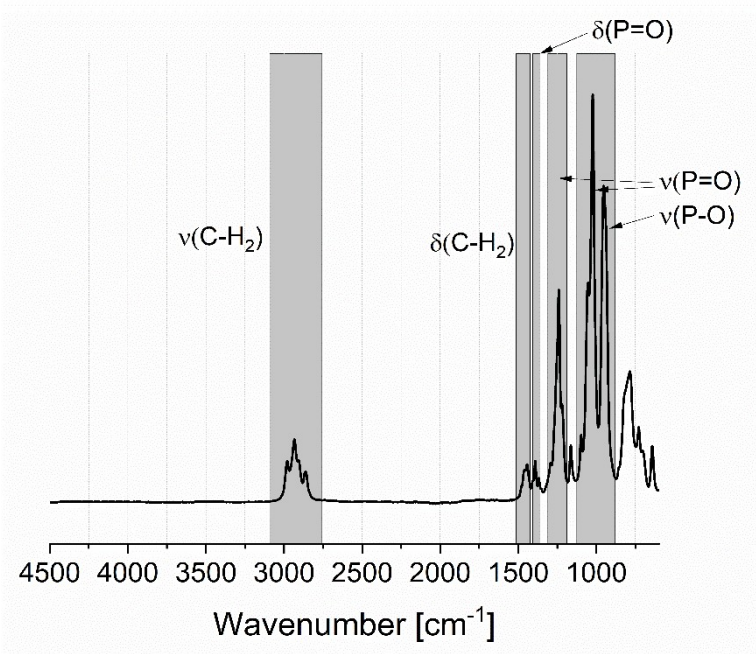

Figure S4: FTIR spectrum of diethyl(6-bromohexyl) phosphonate.

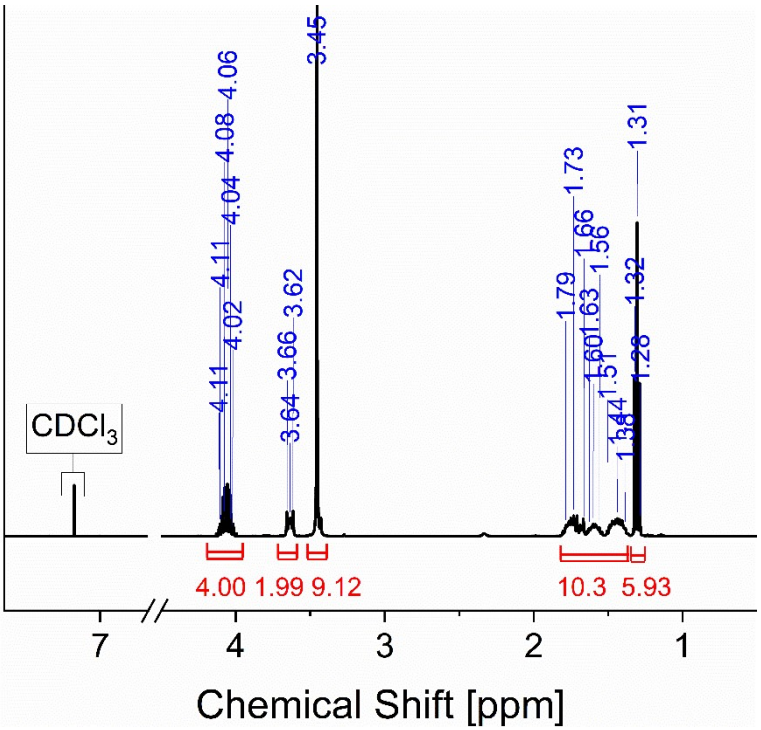

Figure S5: ^{1}H NMR spectrum of 6-(diethoxyphosphoryl)-N,N,N-trimethylhexan-1-aminium bromide.

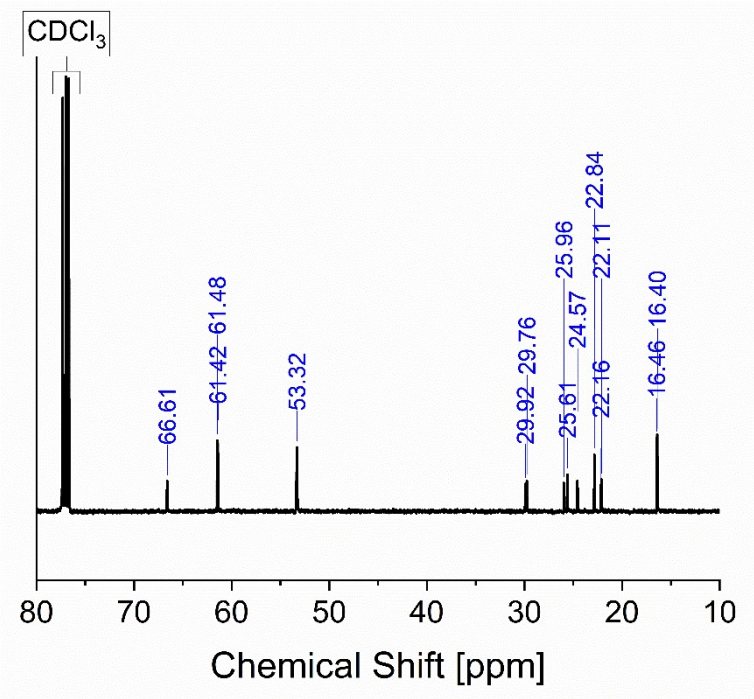

Figure S6: ^{13}C NMR spectrum of 6-(diethoxyphosphoryl)-N,N,N-trimethylhexan-1-aminium bromide.

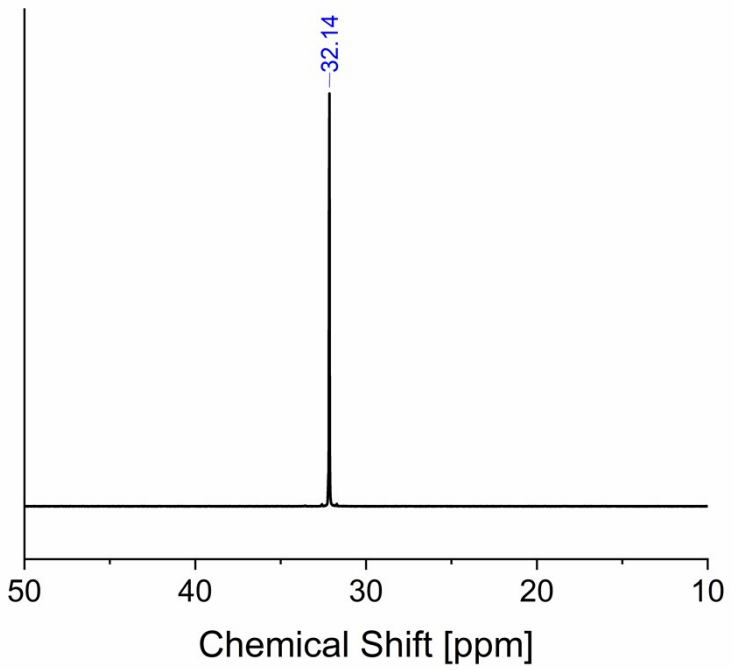

Figure S7: ^{31}P NMR spectrum of 6-(diethoxyphosphoryl)-N,N,N-trimethylhexan-1-aminium bromide.

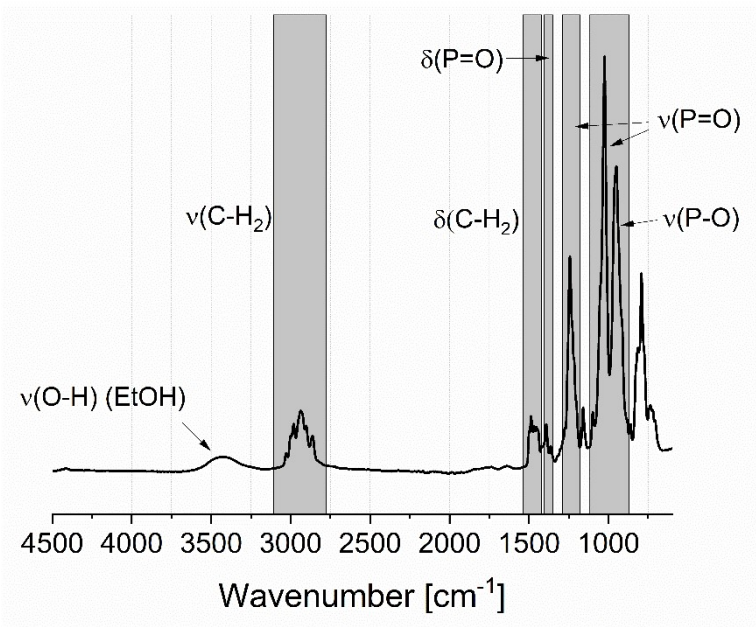

Figure S8: FTIR spectrum of 6-(diethoxyphosphoryl)-N,N,N-trimethylhexan-1-aminium bromide.

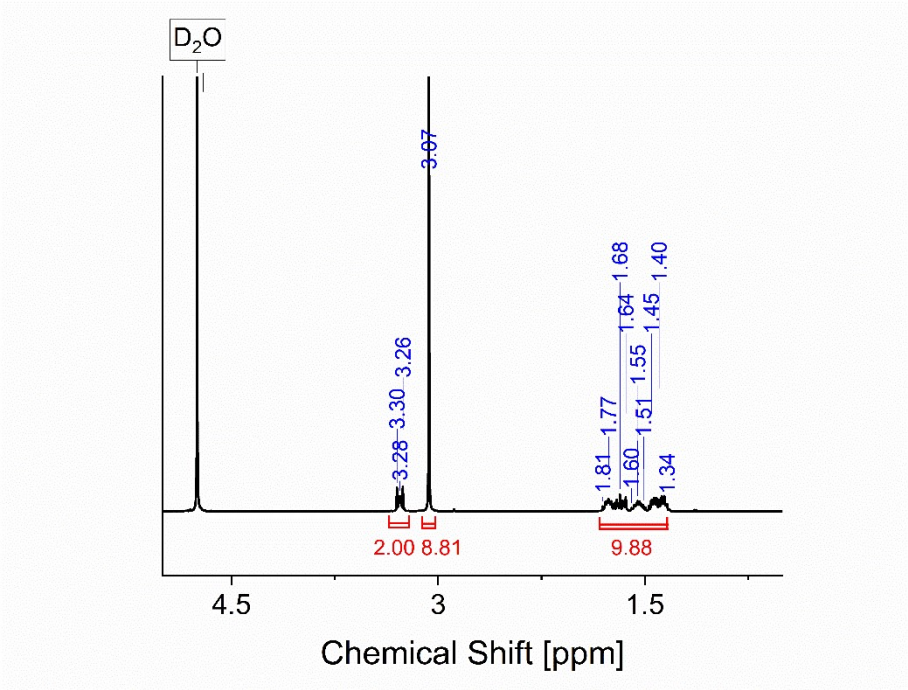

Figure S9: ^{1}H NMR spectrum of N,N,N-trimethyl-6-phosphonhexan-1-aminium bromide.

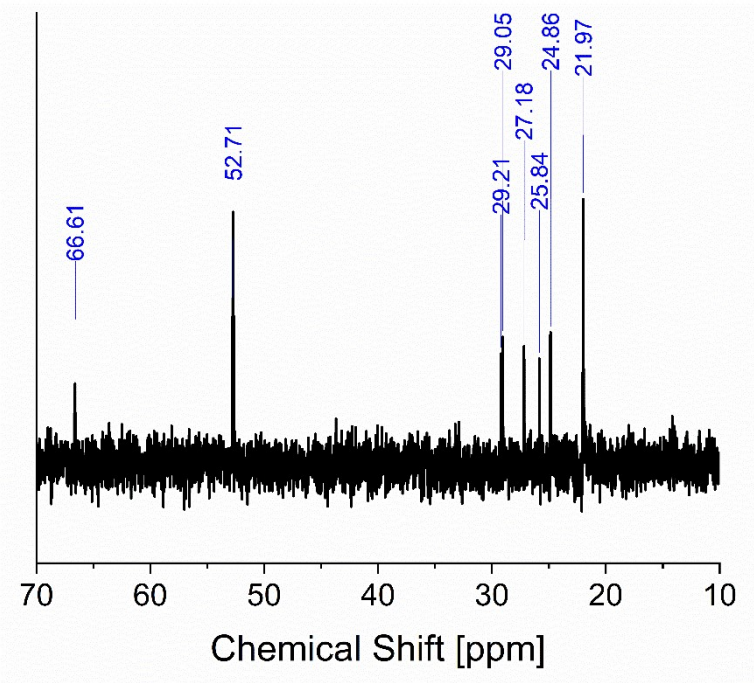

Figure S10: ^{13}C NMR spectrum of N,N,N-trimethyl-6-phosphonhexan-1-aminium bromide.

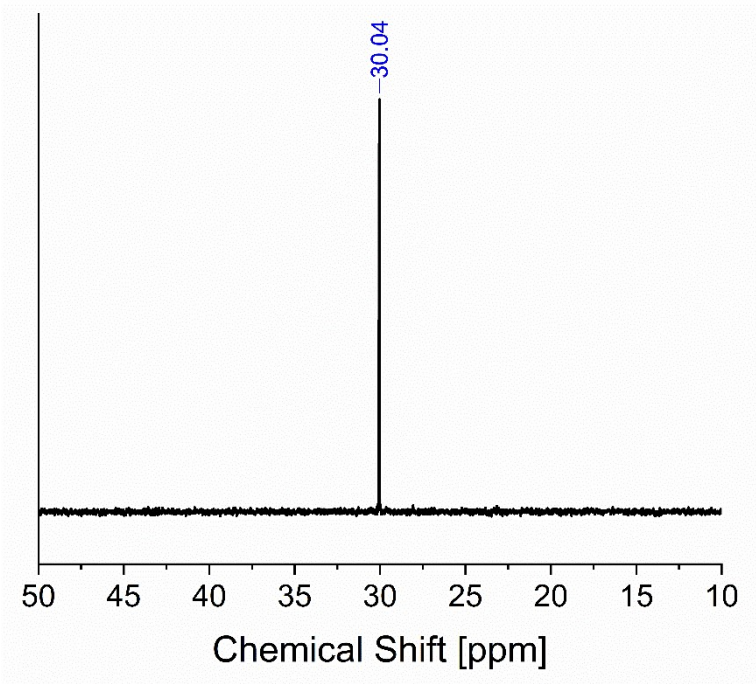

Figure S11: ^{31}P NMR spectrum of N,N,N-trimethyl-6-phosphonhexan-1-aminium bromide.

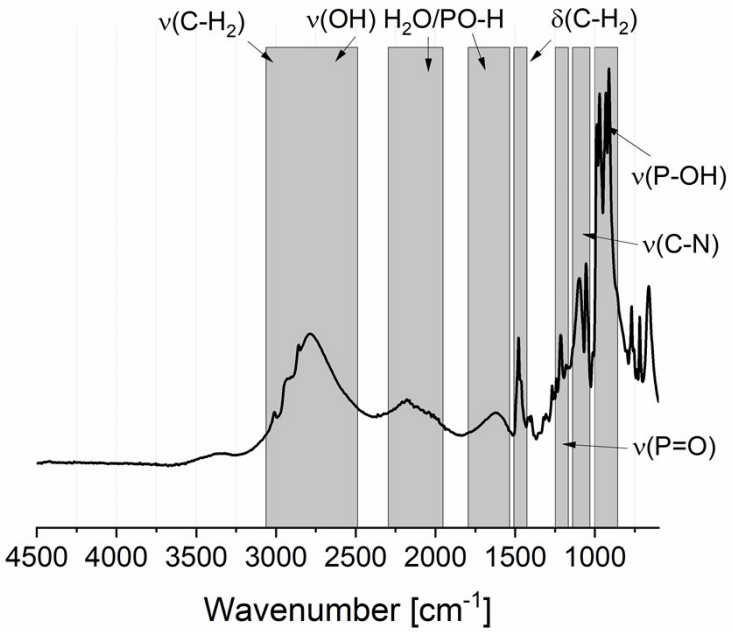

Figure S 12: FTIR spectrum of N,N,N-trimethyl-6-phosphonhexan-1-aminium bromide.

2. NMR and FTIR spectra of sodium 4-(methacryloyloxy)butan-1-sulfonate

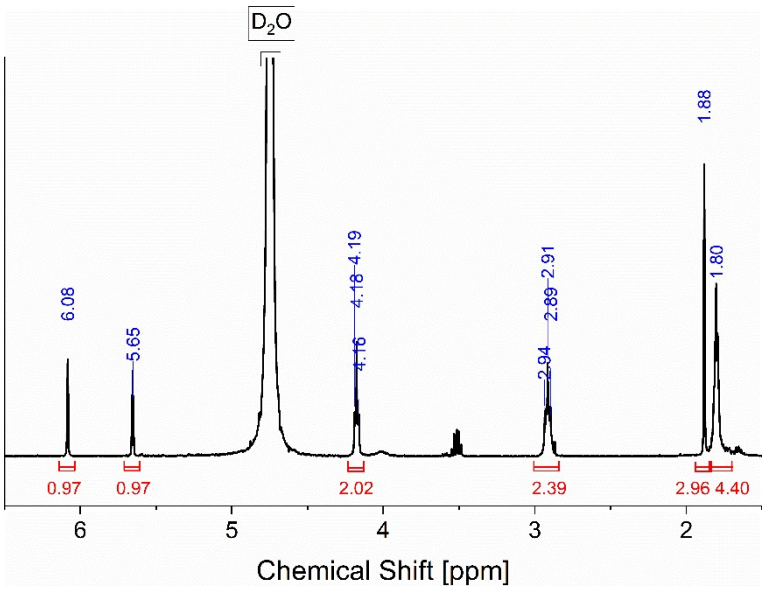

Figure S13: ^{1}H NMR spectrum of sodium 4-(methacryloyloxy)butan-1-sulfonate.

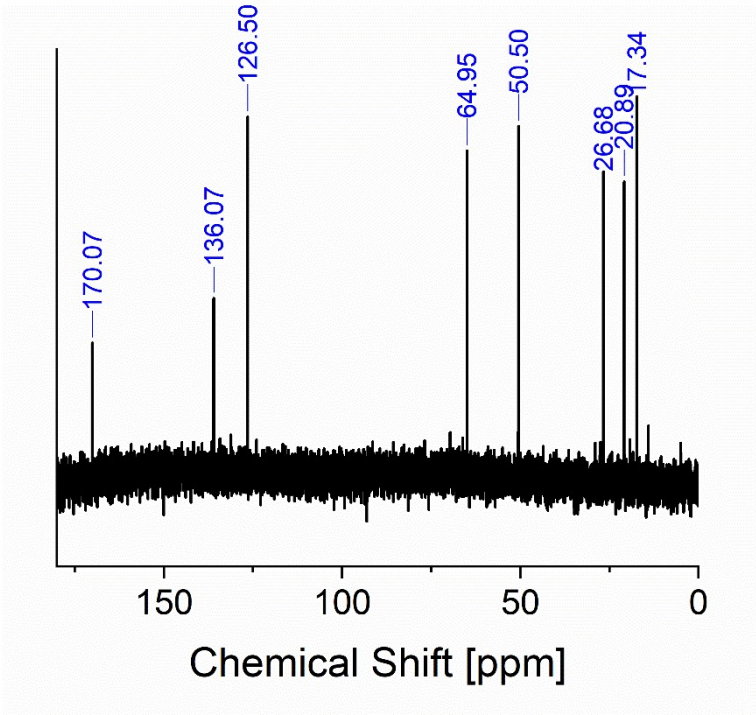

Figure S14: ^{13}C NMR spectrum of sodium 4-(methacryloyloxy)butan-1-sulfonate.

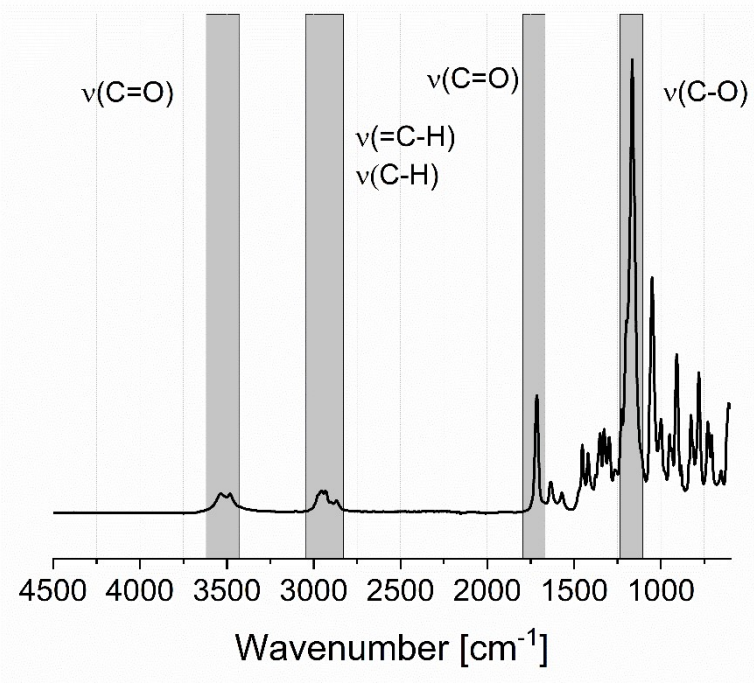

Figure S15: FTIR spectrum of sodium 4-(methacryloyloxy)butan-1-sulfonate.

3. FTIR spectra of the synthesized copolymers

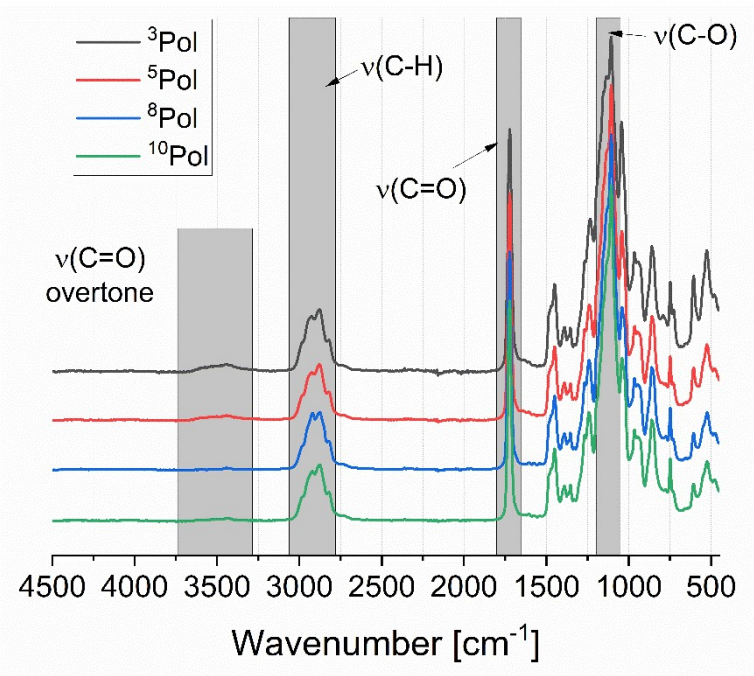

Figure S16: FTIR spectra of the synthesized copolymers.

4. FTIR spectra of the synthesized composites

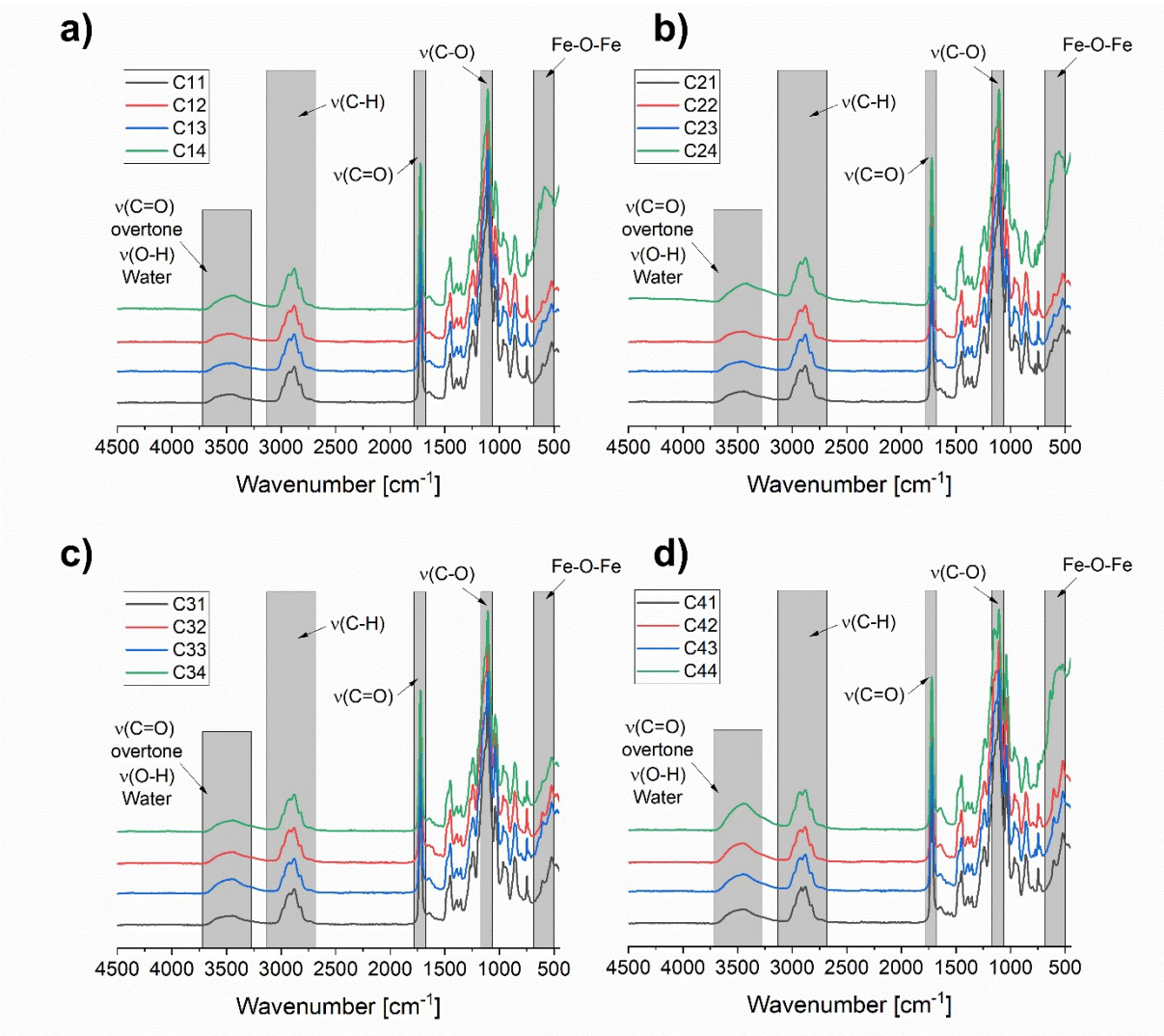

Figure S17: Ir spectra of the a) ^{10}Pol, b) ^{8}Pol, c) ^{5}Pol and d) ^{3}Pol based nanocomposites.

5. FTIR, DLS and TGA measurements of OA@Fe_XO_Y

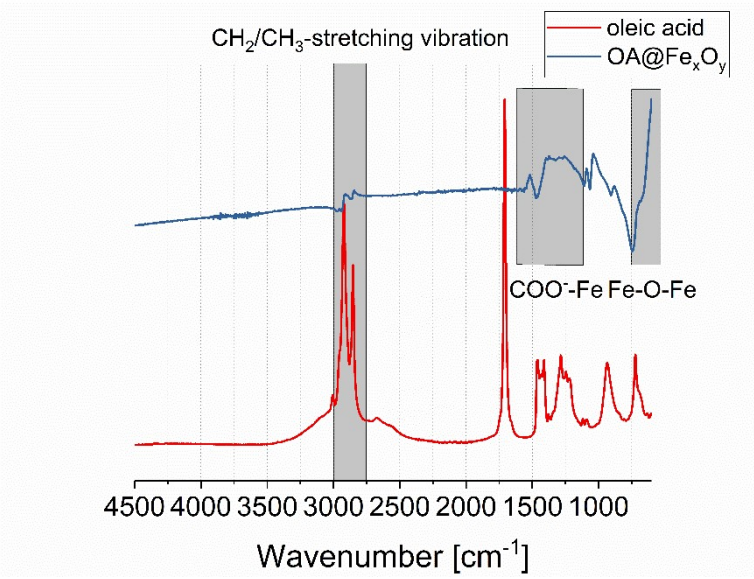

Figure S18: FTIR spectra of Oleic acid (red) and OA@Fe_XO_Y.

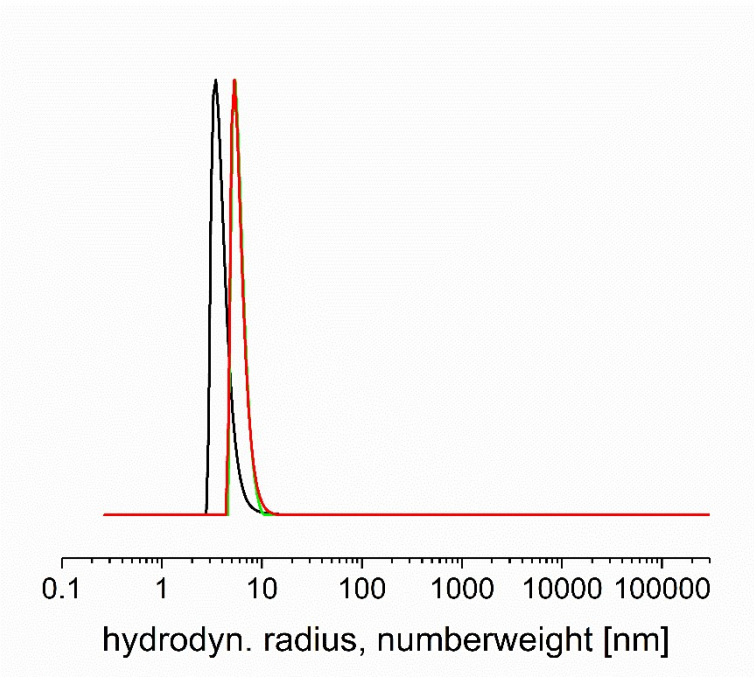

Figure S19: DLS curves of OA@Fe_XO_Y from three different batches in *n*-hexane.

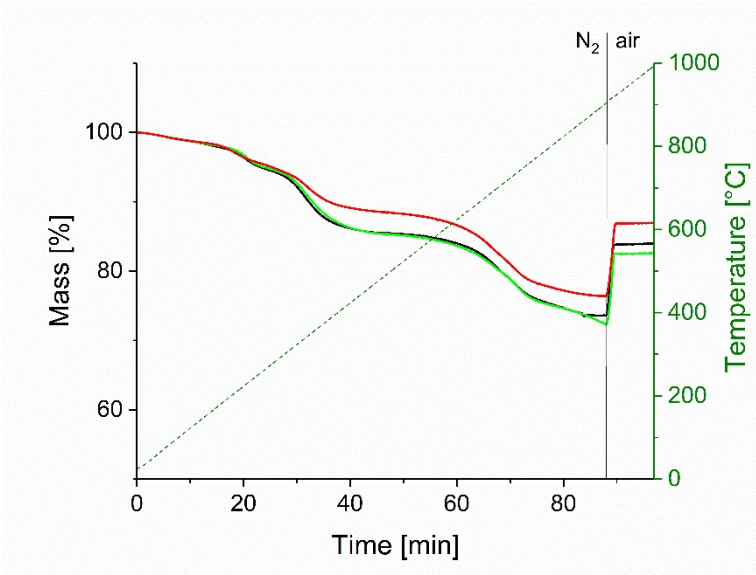

Figure S20: TGA curves of OA@Fe_XO_Y from three different batches.

6. NMR, CHN and TGA data of $^{0.025}$P@Fe_XO_Y - $^{0.600}$P@Fe_XO_Y

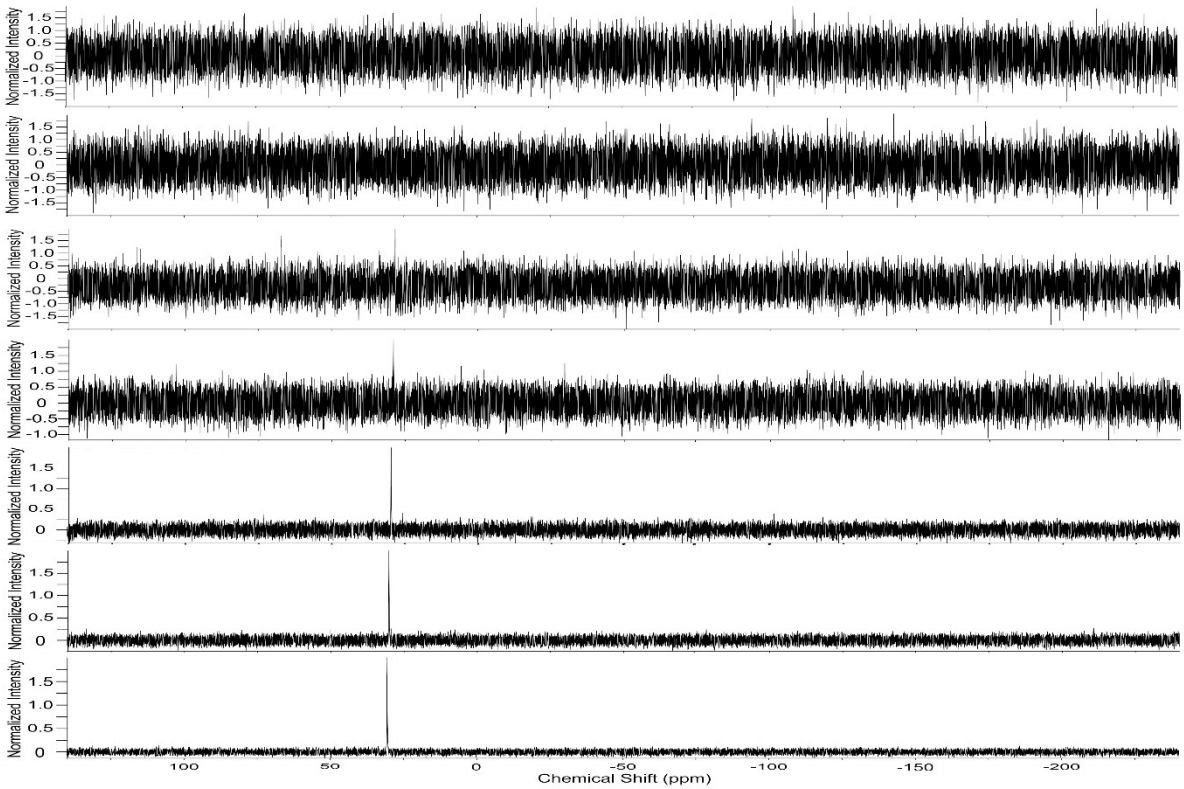

Figure S21: ^{31}P NMR spectra of the supernatant solutions of $^{0.025}$P@Fe_XO_Y - $^{0.600}$P@Fe_XO_Y.

Table S1: TGA and CHN values of oleic acid and the phosphonic acid functionalized nanoparticles.

Sample	TG Residual Mass [%]		CHN [%]			Surface Coverage [mmol/g]		
	25-880°C N_2	880-1000°C air	C	H	N	C	H	N
OA@Fe_XO_Y	80.28	83.41	9.09	1.71	-	0.52	0.62	-
$^{0.025}$P@Fe_XO_Y	78.38	84.95	8.93	1.63	0.48	1.05	0.90	0.44
$^{0.050}$P@Fe_XO_Y	73.71	83.30	9.34	1.88	0.73	1.17	1.10	0.71
$^{0.100}$P@Fe_XO_Y	71.51	81.64	10.45	2.34	0.89	1.35	1.41	0.89
$^{0.200}$P@Fe_XO_Y	69.50	80.68	11.30	2.48	1.00	1.50	1.54	1.03
$^{0.300}$P@Fe_XO_Y	69.04	79.62	11.94	2.51	1.11	1.60	1.57	1.15
$^{0.400}$P@Fe_XO_Y	67.90	79.04	12.31	2.64	1.10	1.68	1.68	1.16
$^{0.600}$P@Fe_XO_Y	66.18	77.84	12.44	2.53	1.26	1.74	1.65	1.36

Table S2: Residual C and H content after subtraction of the phosphonic acid proportion.

C_{exp}	H_{exp}	N_{exp}	C_{phos}	H_{phos}	N_{phos}	C_{resid}	H_{resid}	N_{resid}	$C : H_{resid}$
8,93	1,63	0,48	3,70	0,79	0,48	5,23	0,84	-	6,25
9,34	1,88	0,73	5,63	1,21	0,73	3,71	0,67	-	5,51
10,45	2,34	0,89	6,86	1,47	0,89	3,59	0,87	-	4,13
11,30	2,48	1,00	7,71	1,65	1,00	3,59	0,83	-	4,34
11,94	2,51	1,11	8,56	1,83	1,11	3,38	0,68	-	5,01
12,31	2,64	1,10	8,48	1,82	1,10	3,83	0,82	-	4,66
12,44	2,53	1,26	9,71	2,08	1,26	2,73	0,45	-	6,09

Table S3: CHN values of $^{0.200}P@Fe_XO_Y$ before and after base treatment (pH = 11.5).

Sample	**CHN [%]**		
	C	H	N
$^{0.200}P@Fe_XO_Y$	11.30	2.48	1.00
$^{0.200}P@Fe_XO_Y$ (pH = 11.5)	3.97	1.18	-
OA@ Fe_XO_Y	9.09	1.71	-
OA@ Fe_XO_Y (pH = 11.5)	8.19	1.58	-

7. Investigations on phosphonic acid desorption

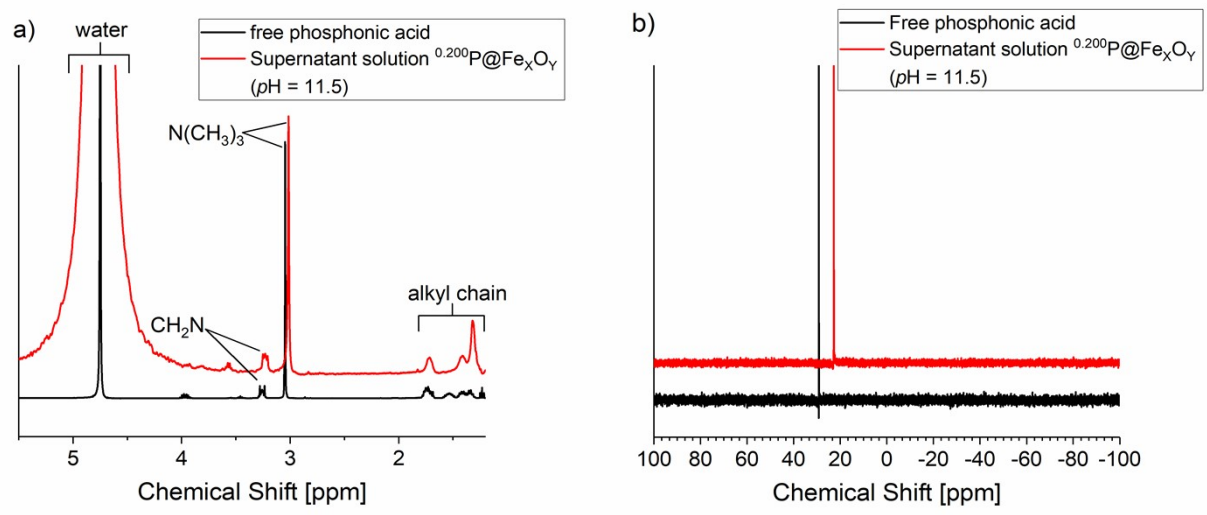

Figure S22: ^{1}H and ^{31}P NMR spectra of the supernatant solution of $^{0.200}P@Fe_XO_Y$ (pH = 11.5) in comparison with the free phosphonic acid.

8. NMR, FTIR and DSC data of the homopolymers

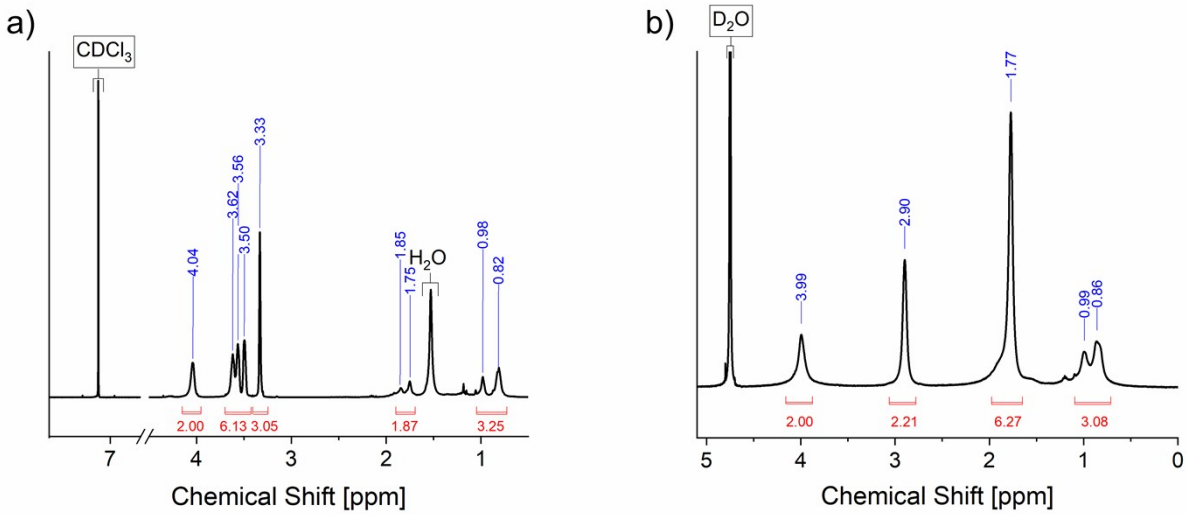

Figure S23: ^{1}H NMR spectra of a) P(DEGMA) and b) P(SMBS).

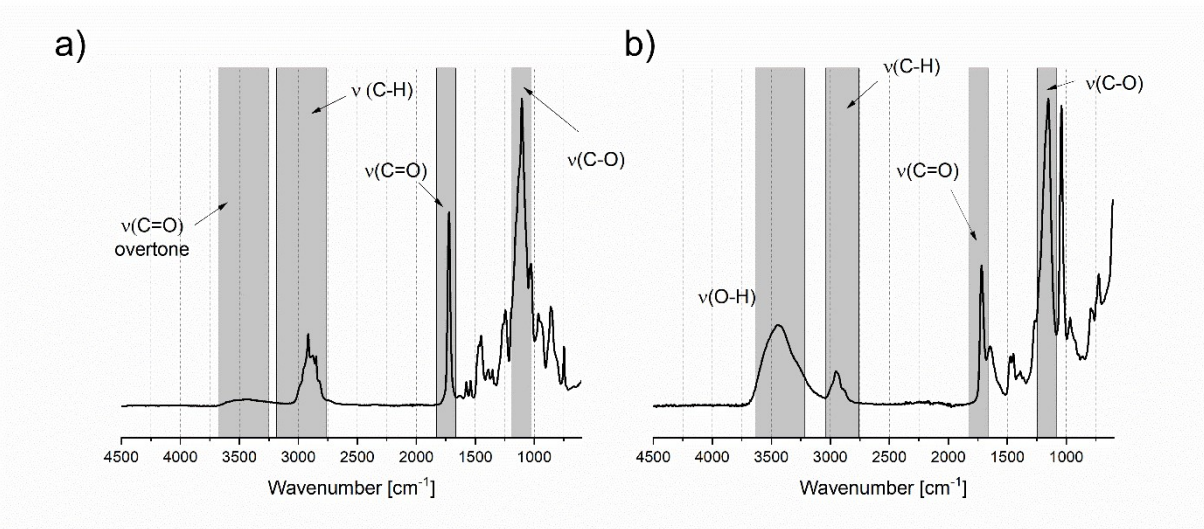

Figure S24: FTIR spectra of a) P(DEGMA) and b) P(SMBS).

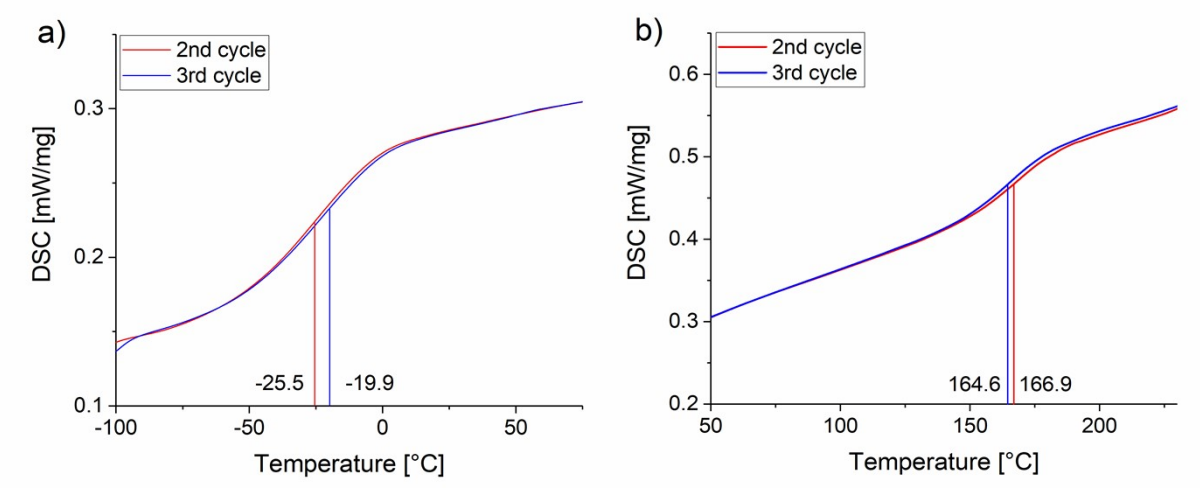

Figure S25: DSC curves of a) P(SMBS) and b) P(DEGMA). T_g determined at $1/2\Delta c_p$.

9. DSC and TGA data of P(SS)

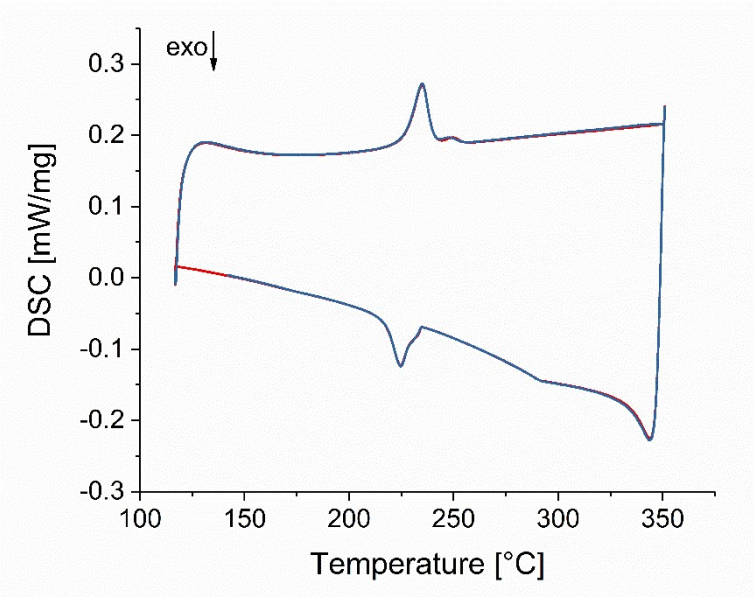

Figure S26: DSC curve of polystyrene sulfonate.

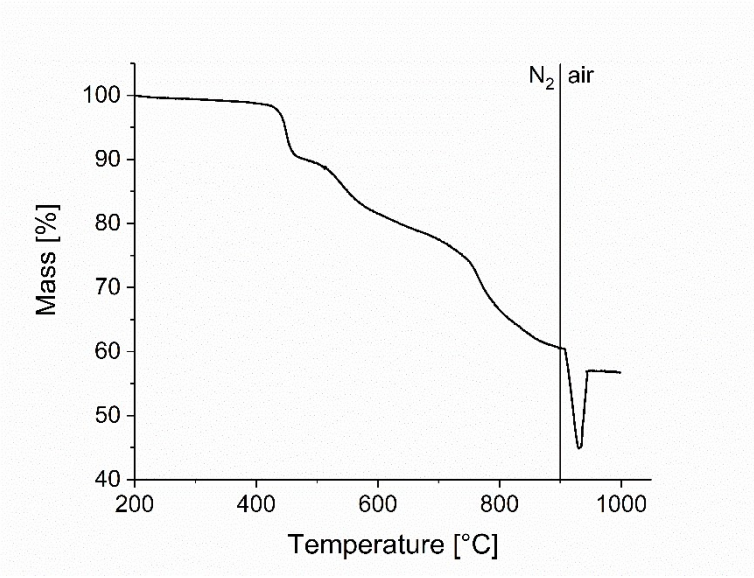

Figure S27: TGA of polystyrene sulfonate.

10. TGA and DSC data of the synthesized composite materials

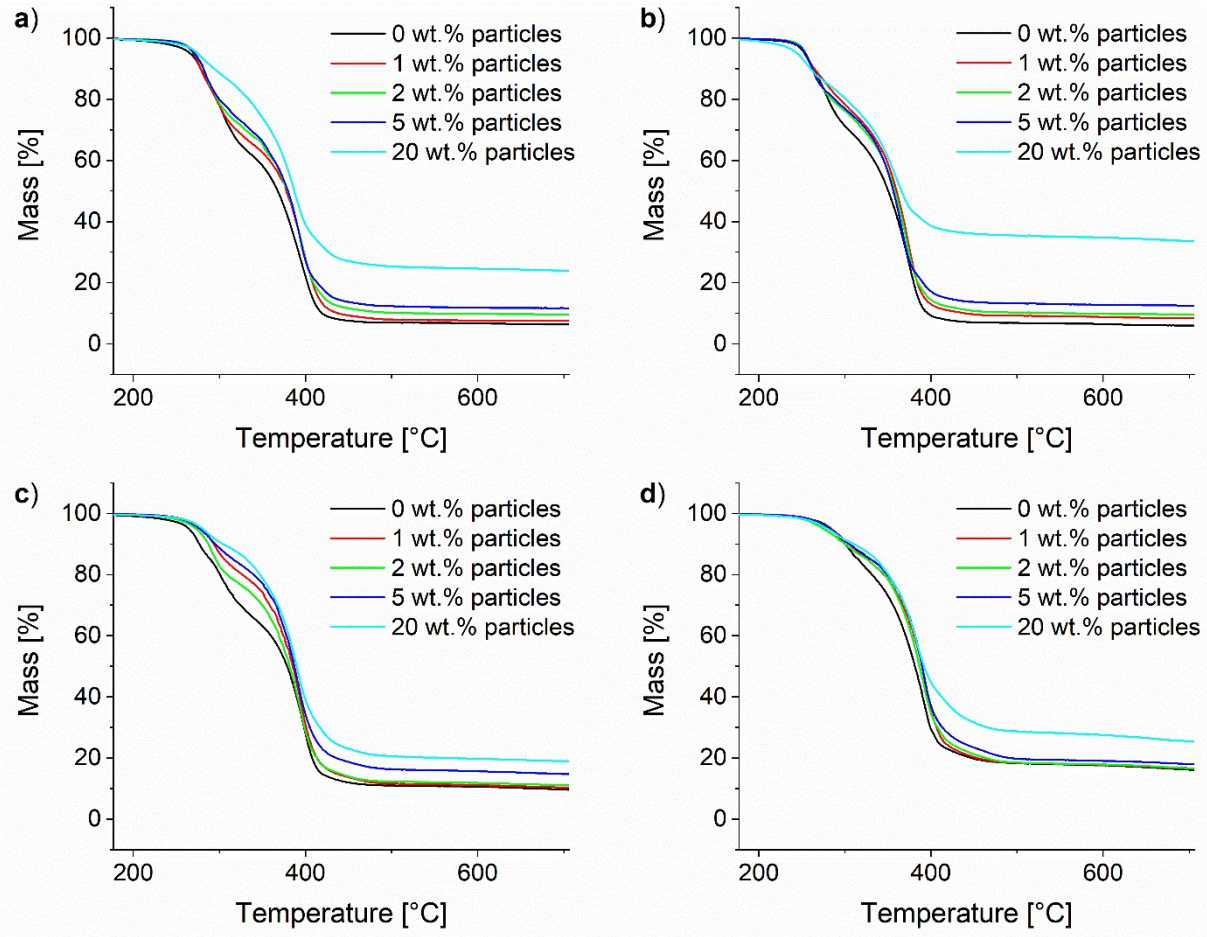

Figure S 28: Thermogravimetric analysis of the synthesized composites. a) ^{10}Pol, b) ^{8}Pol, c) ^{5}Pol and d) ^{3}Pol based systems.

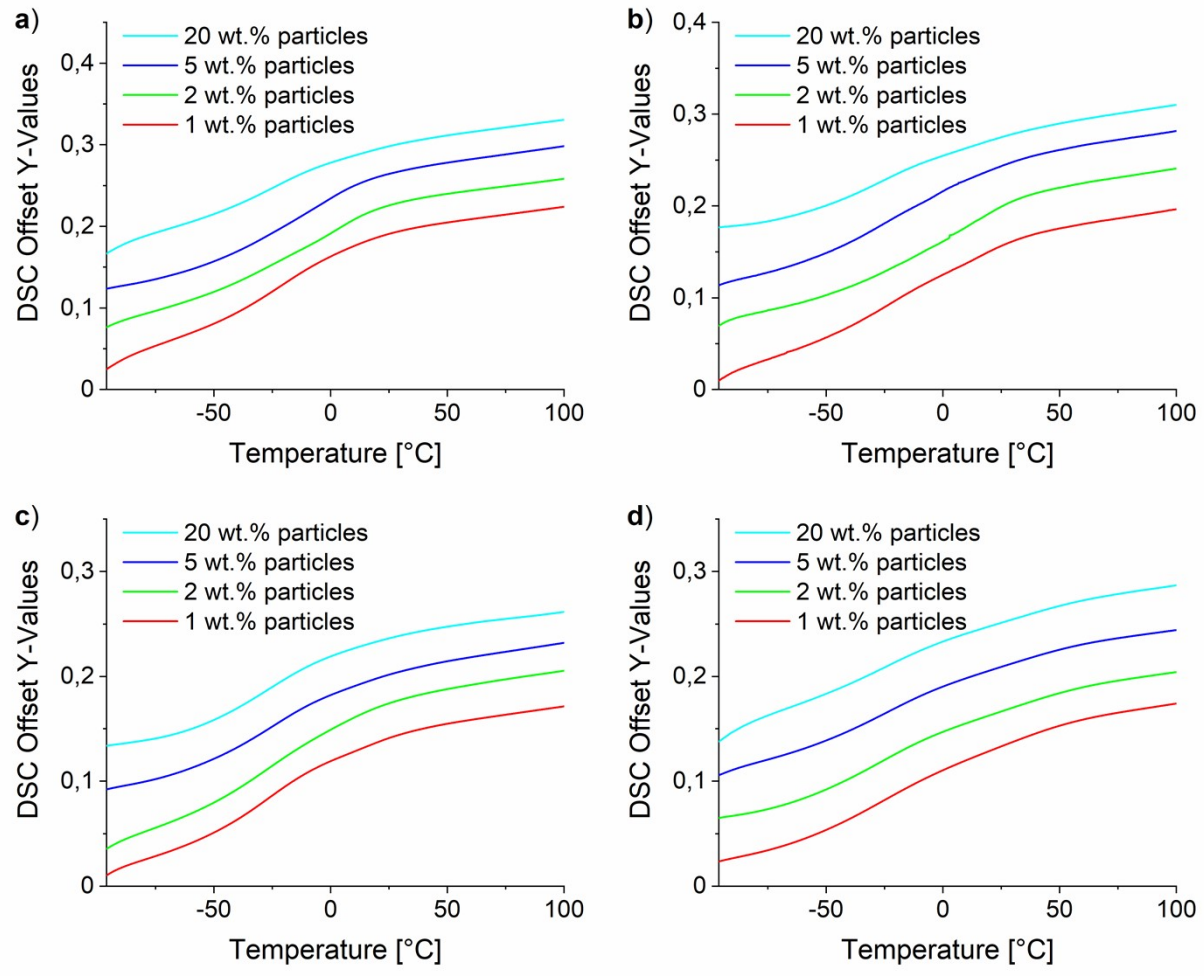

Figure S 29: DSC of the synthesized composites. a) ^{10}Pol, b) ^{8}Pol, c) ^{5}Pol and d) ^{3}Pol based systems.

11. Control experiments for the field induced healing experiments

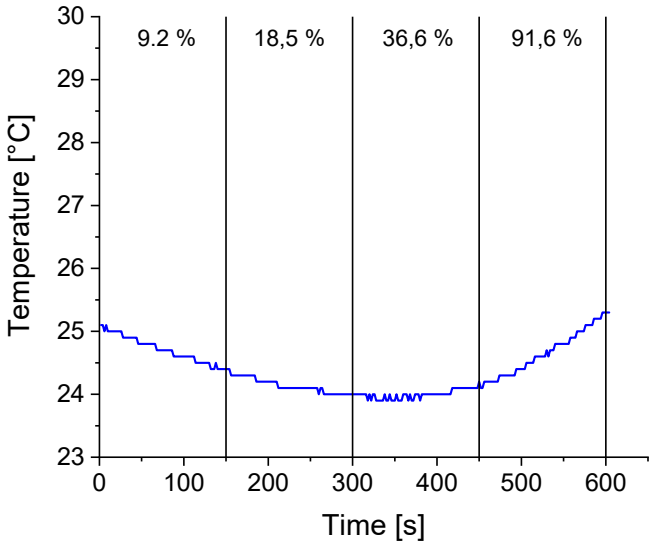

Figure S30: Control heating studies for ^{3}Pol in alternating magnetic fields. Frequency: 313 kHz, percentage values refer to the applied part of the total generator power of 5000 W for the respective heating segment.

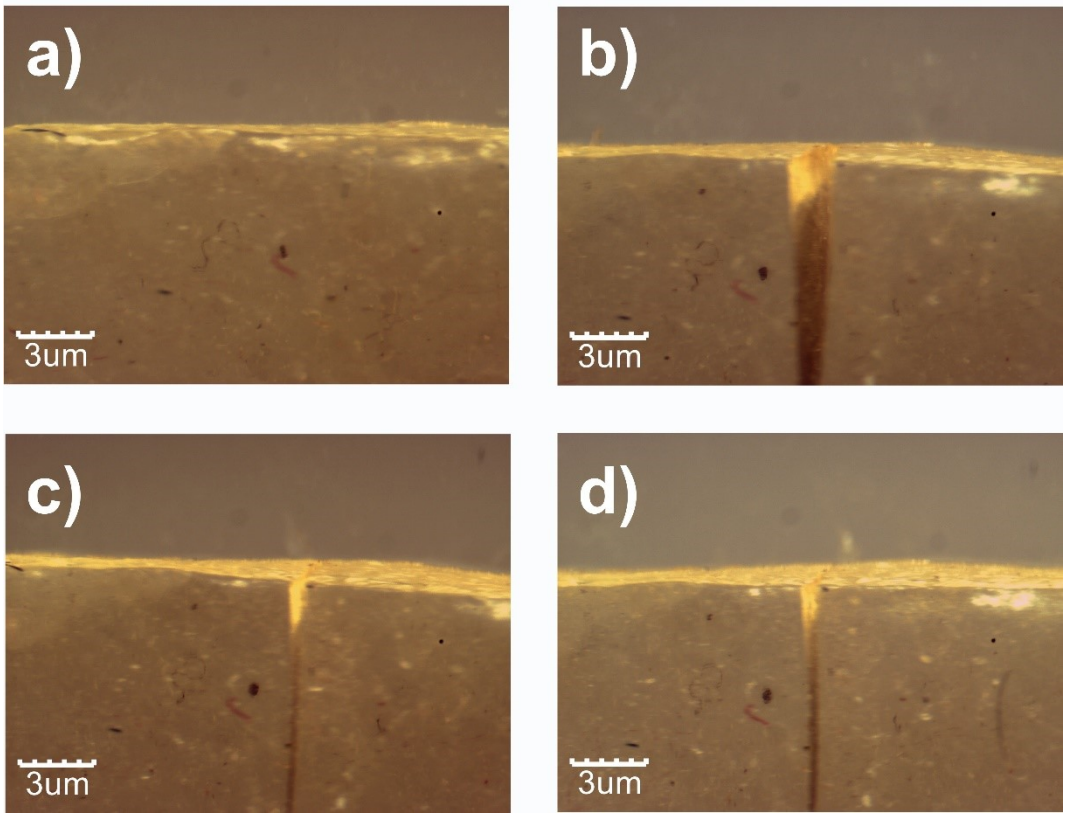

Figure S31: Microscope images of the a) untreated sample ^{3}Pol, b) cut sample, healed sample after c) 24 h and d) 48 h in the induction furnace at a generator power of 4500 W and 313 kHz.